



Distinct phases of eustatism and tectonics control the late Quaternary landscape evolution at the southern coastline of Crete

Mouslopoulou, Vasiliki¹, Begg, John², Fülling, Alexander³, Moraetis, Daniel⁴, Partsinevelos,
5 Panagiotis⁵, Oncken, Onno¹

¹ GeoForschungsZentrum, Telegrafenberg, D-14473 Potsdam, Germany

² GNS Science, PO Box 30368, Lower Hutt, New Zealand

³ Humboldt University of Berlin, 12489 Berlin, Germany

10 ⁴ Sultan Qaboos University, PO Box 36, PC 123, Muscat, Oman

⁵ Technical University of Crete, 73100 Chania, Greece

Correspondence to: Vasiliki Mouslopoulou (vasso@gfz-potsdam.de)

Abstract. The extent to which climate, eustacy and tectonics interact to shape the late Quaternary landscape is poorly known. Alluvial fans often provide useful indexes that allow decoding the information recorded on complex coastal
15 landscapes, such as those of Eastern Mediterranean. In this paper we analyse and date (using optically stimulated luminescence - OSL) a double alluvial-fan system in Crete, an island straddling the forearc of the Hellenic subduction margin, in order to constrain the timing of, and quantify the contributing factors to, its landscape evolution. The studied alluvial system is unique because each of its two juxtaposed fans records individual phases of alluvial and marine incision, providing, thus, unprecedented resolution in the formation and evolution of its landscape. Specifically, our analysis shows
20 that the fan sequence at Domata developed during the last glaciation (Marine Isotope Stage 3; 57-29 kyr) due to five distinct stages of marine transgressions and regressions and associated river incision, as a response to climatic changes and tectonic uplift at rates of ~2.2 mm/yr. Comparison of our results with published tectonic uplift rates from Crete shows, however, that vertical movement on Crete was minimal during 20-50 kyr BP and not uplift was accrued during the last 20 kyr. This implies that eustacy and tectonism impacted on the landscape at Domata over mainly distinct time-intervals (e.g. sequentially
25 and not synchronously), forming and preserving the coastal landforms, respectively.



1 Introduction

Sea-level fluctuations relative to modern sea-level are well constrained for the last 0.5 Ma (e.g., Imbrie et al., 1984; Martinson et al., 1987; Bassinot et al., 1994; Chappell et al., 1996; Dickinson, 2001; Siddall et al., 2003; Rabineau et al., 2005; Lambeck and Purcell, 2005; Antonioli et al., 2007). When these fluctuations are used in conjunction with dating
5 techniques, they provide a powerful tool for interpreting coastal geomorphology and assessing vertical deformation from marine and marginal marine deposits through the middle and late Quaternary (e.g., Pirazzoli et al., 1996; Rabineau et al., 2005; Antonioli et al., 2007; Mouslopoulou et al., 2015a). While there is little debate about the role of tectonic uplift in generating the topographic relief required for the processes of erosion and deposition, uncertainty still exists as to the relative significance of tectonic, eustatic and climatic contributions to deposition and incision of fans of Quaternary age and their
10 variation through time (e.g., Waters et al. 2010).

Alluvial fans are excellent proxies for Quaternary landscape evolution in a climate such as the Mediterranean and their study could potentially place some constraints on the factors that impacted the landscape during its formation and evolution (e.g., Pope et al., 2008; Zacharias et al., 2009). Overall, alluvial-fan deposition is favoured by a rising or relatively high sea-level,
15 and possibly by cold climatic conditions, high rainfall and/or short, intense storms providing enhanced sediment supply and bedload carrying capacity. Alluvial-fan surface abandonment and river incision is favoured by eustatic sea-level fall or tectonic uplift (or a combination of both), reduction in sediment supply due to climatic amelioration or reduced rainfall (e.g., Pope et al., 2008; Waters et al., 2010).

20 This is the case, for example, in southwest Crete (eastern Mediterranean) where Nemeč and Postma (1993) and Pope et al. (2008) studied a fan system and showed that fan deposition was associated with an intense rainfall regime during cold-stage/interglacial transitions, while the tectonic uplift controlled fan incision and provided the required relief. However, we are still unable to precisely understand the interplay between, and the relative importance of, climate and tectonics during late Quaternary in the Mediterranean. Here we capitalise on a well-preserved double alluvial-fan system at Domata in
25 southern Crete (Fig. 1), to study at unprecedented detail the late Quaternary (~50 kyr BP) interplay between sea-level fluctuations and tectonics. The site at Domata is unique on the island of Crete as each of the two juxtaposed terrestrial alluvial fan-building episodes has been followed by individual episodes of alluvial incision and subsequent marine trimming (Figs. 2 and 3).

30 Using luminescence dating together with the international sea-level curve, we find that the alluvial-fan system at Domata was formed during the last ~50 kyr due to five distinct stages of sea-level fluctuations, triggering building of the fans and subsequent river and marine incision, and preserved due to vertical tectonic uplift that allowed the preservation of the fan system from marine inundation.



2 Geological setting of Crete and vertical tectonics

The Mediterranean island of Crete is a mountainous and elongate landmass (~260 km long from west to east, 60 km wide from north to south) that lies within the uplifted forearc section of the Hellenic subduction margin, the most active seismically region in Europe (Fig. 1). The total relative convergence rate between the subducting African Plate and the overriding Eurasian plate is ~35-40 mm/yr (Reilinger et al., 2010). The subduction trench lies ~225 km to the south of Crete (e.g. Ryan et al., 1970; Le Pichon and Anglier, 1979) while the north-dipping subduction interface lies at a depth of ~40 to 65 km beneath Crete (Papazachos et al., 2006; Vernant et al., 2014), with the projection of the down-dip end of the locked zone aligning with the southern coastline of Crete, where the study area is located (Fig. 1) (Meier et al., 2007). The Hellenic Trough, a major bathymetric and tectonic feature within the forearc, lies south of Crete and includes three sections which, from west to east, are named as the Ptolemy, Pliny and Strabo troughs (Fig. 1).

Crete has been characterised by a complex history of vertical movements during Cenozoic (e.g., Peters et al., 1985). Onshore sediments record a period of subsidence and basin development through the Middle and Late Miocene (Serravalian to Messinian) with a change to rapid uplift in the Early Pliocene (Zanclean), followed by slower long-term uplift that continues to the present day (e.g., Le Pichon and Anglier, 1981; Angelier et al., 1982; Meulenkamp et al., 1994; Roberts et al., 2013; Gallen et al., 2014).

Late Quaternary tectonic uplift on Crete is uniform but transient (Mouslopoulou et al., 2015b). Using dated paleoshorelines and numerical models, it is shown that the island of Crete experienced, during the last 20 thousand years, periods of severe uplift (at rates of up to 8 mm/yr) while in the preceding ~30 thousand years, the vertical deformation on Crete was minimal (Mouslopoulou et al., 2015b). Elevated uplift rates (~7-8 mm/yr) are also documented on western Crete since 2 kyr BP, in response to co-seismic uplift (that locally reached up to 10 m) (Pirazzoli et al., 1996; Shaw et al., 2008; Mouslopoulou et al., 2015a). Uplift rate transients on Crete are thought to result from non-uniform stress accumulation and release on upper-plate reverse faults in the overriding plate (Shaw et al., 2008; Stiros, 2010; Mouslopoulou et al., 2015b).

Historical and archaeological records have been also used to link uplift in western Crete to earthquakes (Pirazzoli et al., 1982, 1996; Stiros, 2001; Papazachos and Papazachou, 2003; Papadimitriou and Karakostas, 2008; Shaw et al., 2008; Strasser et al., 2010; Mourtzas, 2012; Stefanakis, 2010). In particular, historic accounts of a major earthquake in Crete in ~AD 365 are approximately coincident with historic documents recording tsunami inundation of parts of the Libyan and Egyptian coastlines, particularly Alexandria (Ammianus Marcellinus, translated by C.D. Yonge, 1862). A gently tilted paleoshoreline (tidal notch) can be followed along the western shoreline of Crete for ~150 km from the area of maximum uplift near the southwest tip (Elafonisi) to as far east as Agios Georgios (Fig. 1). At Domata, our study site, this notch is at 6



m above sea-level. A number of studies have constrained the timing of this prominent paleoshoreline at ~1.5-2 kyr BP, with some attributing it to the 365 AD historic earthquake (e.g., Pirazzoli et al., 1982; 1996; Stiros, 2001; Shaw et al., 2008).

3 Data – Methods - Chronology

At Domata a unique sequence of two individual juxtaposed alluvial fans, each truncated by different episodes of river and marine incision, is documented (see Figs. 2, 3 and 4). The discussion that follows gives a detailed account on the materials and the geometry of the alluvial fan system at Domata and establishes the chronology of its key geomorphic features.

3.1 Coastal geomorphic features at Domata

The landmass of the White Mountains dominates the landscape of western Crete (Figs. 1 and 2). At the southern coastline of Crete, and proximal to our study area, the White Mountains drop abruptly by >1500 m to sea-level, forming a steep and rugged landscape that is often incised by narrow south-dipping gorges (Fig. 2). One such gorge is Klados which reaches the sea at the beach of Domata (Figs. 2 and 3). This steep landscape extends offshore along most of the southwest coast of Crete, as evidenced by the regional bathymetric slopes which are steeper offshore than onshore (Le Pichon and Anglier, 1979; Mascle et al., 1986). As bedrock crops out along much of the southwestern coastline of Crete, it is clear that bathymetric slopes are also cut in bedrock, implying that the Quaternary sediment sequence recorded at Domata has no significant thickness offshore.

The rivers within the gorges of western Crete are usually ephemeral and scour to bedrock, depositing gravels only locally, commonly where valleys widen at junctions with side valleys or close to the coast. As the rivers approach the sea, gradients shallow and stream carrying capacity decreases resulting in deposition from bedload of fans grading to the shoreline. The headwaters of the Klados River reach an elevation of ~1600 m in the White Mountains. In the Domata area bedrock comprises limestone of the Tripolitza Group of Carboniferous-Permian age (Christodoulou and Tataris, 1969).

In order to better interpret the geomorphology at Domata we topographically surveyed and modelled the entire study region (Figs. 3 and 4). The data acquisition was performed with a double precision Real Time Kinematic (RTK) GPS receiver and was readily corrected to provide coordinates under the Greek Geodetic Reference system (GGRS 87). The topographic dataset includes a total of 4,156 survey points, measured under an excellent geometric dilution of precision (GDOP) and accuracy of <1 cm. Some areas were not surveyed due to dense vegetation; however, values for these regions were interpolated using the 'nearest neighbour method'. A series of breaklines and sparse elevation models from the National Cadastre and Mapping Agency of Greece were incorporated in the model (Fig. 4a) to optimise representation.

30



At Domata, two triangular, elevated fan surfaces covering a combined surface area of $\sim 0.1 \text{ km}^2$ near the mouth of Klados River, rise to an inland elevation of $\sim 100 \text{ m}$ (Figs. 2, 3 and 4). These fan surfaces are unique in south Crete as they are protected from alluvial erosion by a low bedrock ridge (Fig. 2) which channels the river flow to the western side of its narrow valley. Where the Klados River leaves its bedrock gorge, $\sim 600 \text{ m}$ from the coast, its channel is incised into gravels
5 $\sim 40 \text{ m}$ below an abandoned (lower) fan surface (Figs. 2 and 3). The gravel on lapping occurs without any deformation (e.g., faulting) on the bedrock landscape. Downstream, $\sim 40 \text{ m}$ from the river mouth, the seaward extent of the lower-fan surface is at c. 35 m above sea-level (Fig. 4). Here, the fan surface and its alluvial entrenchment cliff are trimmed parallel with, and close to, the present shoreline (Figs. 2 and 3). The linearity and parallelism of this cliff to the modern coastline clearly implies that this cliff has been trimmed by the sea. The elevation of the lower-fan surface decreases eastwards along the sea-
10 trimmed cliff to $< 10 \text{ m}$ above sea-level near the east end of Domata beach (Figs. 2 and 5). Along this coastal cliff, the highest elevation of the fan is $\sim 90 \text{ m}$ east of the Klados River (Figs. 2 and 5).

The upper-fan surface is at $\sim 100 \text{ m}$ elevation at its upstream extent, $\sim 60 \text{ m}$ above the active river and $\sim 20 \text{ m}$ above the lower-fan surface (Figs. 4 and 5). The upper-fan deposits are truncated by an old river incision (trending $\sim 200^\circ$) that is older than
15 the lower-fan surface, as the deposits of the lower-fan lap against the buried upper-fan deposits (Fig. 3). Downstream, the seaward extent of the upper-fan surface and its entrenchment cliff are truncated by another marine cliff (trending $\sim 130^\circ$) that pre-dates deposition of the lower-fan, as the lower-fan surface also laps against this (Figs. 2 and 3). Where the marine trimming truncates the upper-fan surface and its entrenchment cliff, the surface has an elevation of c. 60 m , decreasing eastwards to $\sim 30 \text{ m}$ at the east-end of the beach (Figs. 2, 4 and 5). In the east, the upper-fan is overlain by silty sand near the
20 eastern end of Domata Beach. This is the only stream gully that crosses the fan surfaces, draining the bedrock area behind the fans; this ephemeral stream is probably the source of the silty sand (UF-2 sample in Table 1).

Lower-fan materials exposed in the sea-cliff are dominantly poorly sorted gravels, moderately stratified, with coarser beds commonly $< 2 \text{ m}$ thick and finer beds $< 1 \text{ m}$ thick that display lateral lensing and channelling (Fig. 6a). Bedding is convex
25 up, sub-parallel with the lower-fan surface. Some individual beds can be traced laterally up to $200\text{-}300 \text{ m}$ (see thin dashed lines in Fig. 6a). In the coastal cliff, the abandoned surface of the lower-fan materials lap onto a gently undulating, sub-horizontal discontinuity on an underlying older alluvial gravel (e.g. remnants of the upper-fan) that is significantly coarser with a higher fine-grained content (Figs. 2, 3 and 6a). The contact surface between the two fan units is very clear and extends along the length of the beach (Fig. 6a) and also up the Klados River for $\sim 100 \text{ m}$ (Fig. 3). Only in places the contact may be
30 locally obscured by fallen debris, but it is clearly subhorizontal, with low relief and undoubtedly separates the two fan units (Fig. 6a).

Other subtle geomorphic feature of interest is an intertidal bioerosion notch in bedrock, stranded $\sim 6 \text{ m}$ above present sea-level at the west end of Domata beach (Fig. 6b). This notch continues west and east from Domata and has been mapped



around the coastline of western Crete and attributed to a seismically uplifted paleoshoreline dated at ~1.5-2 kyr BP (e.g., Pirazzoli et al. 1982, 1996; Shaw et al. 2008; Mouslopoulou et al., 2015a). The presence of a small terrace on the west side of the Klados River (Fig. 6b) at approximately the same elevation (6m) represents an alluvial terrace stranded by that uplift. As with the lower-fan, this terrace has been trimmed by the sea. This late-stage uplift resulted in a readjustment of the Klados River bed and incision near the mouth of the stream (Fig. 6b).

Further, older geomorphic features are also present at Domata: two marine terraces, elevated at about 100 and 360 m respectively, are cut on the south-facing mountain, west of the Klados River (Fig. 2). While we cannot assign ages to these benches, their altitude and geomorphic similarity with known and dated late Pleistocene marine benches elsewhere in Crete (e.g. Shaw et al., 2008; Strasser et al., 2011; Strobl et al., 2014; Mouslopoulou et al., 2015a), provides some stratigraphic and chronologic context for the age of the alluvial fans at Domata (i.e., the alluvial fans, which have lower altitude compared to these marine terraces, are expected to be younger than 125 kyr).

3.2 OSL dating of alluvial fans

To place chronologic constraints on the series of geomorphic features established at Domata, we collected in steel tubes five samples for OSL dating from depths ranging from 0.24 to 1.1 m below the ground surface (Table 1). One sample is collected from the surface of the upper-fan (UF-1) to constrain the end of the upper-fan aggradation (surface abandonment) and the initiation of incision (Fig. 3). A further sample (RB-1) is collected from the upper-fan deposits exposed in the lower reaches of the Domata stream cliff to constrain the age of deposition of the early upper-fan deposits (Fig. 3). Two samples are collected from the lower-fan surface (LF-1a/b and LF-2a/b) to provide constraints on the timing of lower-fan abandonment and initiation of incision (Fig. 3). A further sample (UF-2) is collected from deposits (silty sand) mantling both the lower and upper-fan to test its age relative to UF-1 and UF-2. The results of the OSL analysis are presented in Table 1 and Figure 7.

3.2.1 Sample preparation and measurements

All samples were dated in the luminescence lab at Humboldt University of Berlin (Germany). All sample preparation steps were conducted under subdued red light according to standard procedures. After separating the wanted grain size fractions by wet sieving (38-63 μm and 90-200 μm), carbonates and organic material were removed using 10% hydrochloric acid and 10% hydrogen peroxide. Quartz and potassium feldspar were extracted from the coarser grain fraction by density separation using heteropolytungstate heavy liquid (LST) of 2.75, 2.62 and 2.58 g/cm^3 . The subsequent etching of the separated quartz with hydrofluoric acid (40%, 60 min) eliminated any potential feldspar contamination and removed the alpha irradiated outer grain layer. From the finer fraction of 38-63 μm quartz was isolated by a two-week treatment with 38% hexafluorosilicic acid. After renewed sieving small multiple grain aliquots (2mm) were prepared of etched quartz (90-200 and 38-63 μm) and potassium feldspar (90-200 μm).



Quartz OSL (optical stimulated luminescence) measurements were performed on a Risø TL/OSL-DA 15 reader (blue LED stimulation at 470 nm and detection through a Hoya U340 filter with transmission centered on 330 nm) and on a Lexsyg luminescence measurement system (green LED stimulation at 525 nm and detection through a Schott BG3 Delta-BP365/50 EX-Interference filter combination at 380 nm). Feldspar IRSL (infrared stimulated luminescence) measurements were conducted on a Lexsyg luminescence measurement system (IR-LD stimulation at 850 nm and detection through a Schott BG39 AHF-BrightLine HC 414/46-Interference filter combination at 410 nm). Quartz paleodoses were measured using a SAR (single aliquot regenerative) protocol according Murray and Wintle (2000, 2003) with preheat temperature set to 240°C (10s) and test dose cutheat to 160°C. Wallinga et al. (2000) introduced the SAR protocol to the IRSL dating of potassium feldspar. It was here modified following Blair et al. (2005) applying equal preheat procedures after every irradiation step (250°C, 60s). The appropriate preheat temperatures and durations were identified conducting dose recovery tests on samples RB-1 and LF-2a/b (SAR equivalent dose determinations of known lab doses with varying preheat temperatures). Quartz was stimulated at 125°C for 40 s, feldspar at 50°C for 300 s. The built-in beta sources (Sr-90) emitted 0.068 Gy/s (Lexsyg) and 0.093 Gy/s (Risø) respectively. The sediment dose rates were estimated by measuring the contents of uranium, thorium and potassium on a high resolution gamma spectrometer. The cosmic-ray dose rates were estimated from geographic position, elevation and burial depth (Prescott and Hutton, 1994). The internal potassium content of the measured feldspar was assumed to be 12.5 ± 0.5 % according to Huntley and Baril (1997).

3.2.2 OSL results

Quartz OSL dating results reported in Pope et al. (2008) proved the suitability of standard quartz SAR protocols for dating fan sediments along the nearby Sfakia piedmont in southern Crete (Fig. 1). In contrast, the investigated quartz from Domata showed bad luminescence properties: the OSL signals were dim, dose recovery tests yielded poor results, the highly scattering paleodoses produced positively skewed broad distributions and the resulting quartz ages showed no stratigraphic reasoning (underestimation of true age). This led to the conclusion that quartz is not the proper material for dating the alluvial fans at Domata. The most likely explanation for the non-suitability of the quartz (weak, or even missing, fast OSL signal component) is the dominance in our samples of fresh insensitive quartz, which had undergone only few sedimentation cycles (Preusser et al. 2006; Steffen et al., 2009). Thus, potassium-feldspar (IRSL) was used instead to date the landforms at Domata.

The feldspar (IRSL) dating produced reliable age ranges (Fig. 7). Best results for dose recovery tests on laboratory-bleached feldspar samples from Domata were obtained without applying any sensitivity correction. Thus, a simplified SAR protocol without testdose measurements was used for the paleodose determination of the natural potassium-feldspar samples. No fading tests were made to correct for any potential age underestimation. Sensitivity changes were assessed by repeating the first irradiation step at the end of each SAR cycle assuming that the luminescence intensities should coincide (recycling ratio



close to 1.0). Here, a recycling ratio between 0.85 and 1.15 was tolerated. The a -value for assessing the alpha particle contribution to the paleodose was set to 1.5 ± 0.5 (Balescu and Lamothe, 1994). Basic statistic values are presented in Table 1. Under perfect conditions the arithmetic mean and the median should coincide. But here the mean value is always larger compared to the median, typical for positively skewed age distributions. This can indicate insufficient exposure of the sediment to daylight during the last sedimentation cycle. But also post-depositional mixing, contamination with younger grains from the surface (low sampling depth, bioturbation) or microdosimetric inhomogeneities are possible reasons for skewed age distributions. Compared to the mean, the median is less sensitive to large outliers (RB-1, LF-1a/b) while the peak of the kernel density estimation (KDE_{max}) reflects the value with the highest probability within the distribution applying a fixed bandwidth (Galbraith and Roberts, 2012).

10

Collectively, our potassium-feldspar measurements suggest that the age of the landforms at Domata ranges between ~55 and 25 kyr BP (Table 1). Thus, the chronostratigraphy of the majority of the geomorphic landforms formed during MIS 3 (29-57 kyr). When used in conjunction with the international sea-level curve (e.g., Siddall et al., 2003), the chronology of the geomorphic events that formed the landscape at Domata can be established reasonably well, despite the significant errors in the OSL measurements (Fig. 7). The landscape evolution, including its chronology, is discussed in Section 4.

15

3.3 Soil development

We have performed a macroscopic soil-profile characterization for the soil-horizons that develop on the two fan surfaces (Fig. 8a). The fan surfaces are generally flat, with a maximum gradient of $\sim 7^\circ$ and incision restricted to few dry and shallow (<1m) creek courses. Thus, erosion on these surfaces is expected to be minimal. Nevertheless, to minimise the effect of soil erosion, we located our soil-profiles away from creek incisions.

20

The soils at Domata are categorized as Leptosols (Soil Atlas of Europe, 2005; FAO, 2006) and comprise a shallow (<0.5 m) soil cover over coarse sediment of highly calcareous material (Fig. 8). Both soils have common parent material, mainly consisting of limestone pebbles and cobbles, and are covered by pine trees (*Pinus brutia*) (Fig. 8a). The soils in the upper (UF) and lower (LF) fans differ macroscopically and biochemically in physical and geochemical parameters. Soil thickness varies from 0.1 m (Fig. 8b) on the lower-fan to 0.4 m (Fig. 8c) on the upper-fan (measurements are averaged from a total of 6 soil profiles). The UF soil is yellowish-brown with A and (weak) B horizons and texture from subangular to granular while the LF soil is yellowish with granular texture and has no distinct horizons (apart from a very thin horizon A) (Fig. 8b and c).

30

Comparison of the macroscopic characteristics of the soils at Domata with the soils identified at the piedmonts at the nearby region of Sfakia (Fig. 1) by Pope et al. (2008), provides additional evidence that the alluvial fan system at Domata was formed during MIS 3 (as constrained by the OSL dating). Specifically, at Domata we find soils the characteristics of which



closely resemble the soils that developed at Sfakia during stage 2C (70-16 kyr BP), while there is total absence of older soils that developed during stage 2A (~144 kyr) (Pope et al., 2008). The former (stage 2C) is a brown to yellowish-brown soil with limited B horizon and subangular texture, characteristics that match the soils at Domata, whereas the latter contains highly crystalline iron oxides with a clear B horizon.

5

The macroscopic observations (UF soil thicker and redder) also imply that the upper-fan soil is more mature compared to that of the lower-fan. Preliminary geochemical analysis (Moraetis et al., 2015) confirms that the soil in UF is more mature (e.g., older), as it has lower *specific surface area* and higher content of well-shaped hematite (and less goethite) compared to that in the LF (Wang et al., 2013). This observation is also in agreement with soil analysis at the nearby region of Sfakia (Fig. 1), where Pope et al. (2008) showed that the soil redness and the content of crystalline iron oxide (hematite) increase with increasing alluvial fan age. The greater age of the UF soil compared to the LF soil is also independently confirmed by our observations on crosscutting and incision of fans and the OSL dating that shows that the lower-fan developed at least 5 kyr earlier than the lower (see discussion in Section 4; Table 1). According to Lair et al. (2009), the ~5 kyr of difference in the residence time between the two soil horizons is sufficient to generate the recorded macroscopic and geochemical changes.

15

4 Landscape evolution at Domata

The sequence of events that resulted in the development of the landscape at Domata, as supported by the superposition of the luminescence dating onto the international sea-level curve of Siddall et al. (2003) (Fig. 9) and the analysis of the geomorphic landforms (Fig. 10), is as following (from old to young): *a*) deposition of the upper-fan materials (Fig. 10a); *b*) river incision leading to abandonment of the upper-fan surface (Fig. 10b); *c*) marine trimming of the upper-fan surface, the fan deposits and the river-incision cliff (Fig. 10c); *d*) deposition of the lower-fan surface against the upper-fan alluvial cliff and upper-fan sea-cliff (Fig. 10d); *e*) river incision leading to abandonment of the lower-fan surface (Fig. 10e); *f*) marine trimming of the lower-fan surface, the fan deposits and the incision cliff (Fig. 10f); *g*) seismic uplift resulting in a stranded paleoshoreline, the development of a river terrace riser and the oversteepening of the lower river channel (Fig. 10g). In the following discussion we provide evidence in support of each stage of the landscape evolution at Domata and we establish its chronology.

25

The initiation of deposition of the upper-fan (Fig. 10a) is likely to have occurred post ~50 kyr BP and prior to 45 kyr (median of RB-1 sample; Table 1). This period coincides with a cold period of falling sea-level that promotes deposition (sea-level reached c. -92 m at 45 kyr; Fig. 9). We argue that upper-fan deposition is unlikely to have started as early as 53.4 kyr (mean of RB-1 sample; Table 1) because there is no geomorphic evidence (e.g., marine cliffs) to record the two subsequent high sea-level stands at c. 45 and 39 kyr. Thus, the deposition of the upper-fan postdates 53 kyr and is completed

30



by ~45 kyr BP, when sea-level rose to reach at c. -72m. The period that follows, between 45-41 kyr, reflects an increasingly cooler climatic period with possible increase in sediment supply, and a falling sea-level to -87 m (Fig. 9). During this period, alluvial-fan incision took place forming an alluvial cliff entrenchment (Fig. 3) and the upper-fan was eventually abandoned (Fig. 10b). This period was followed, at ~39 kyr BP, by a marine transgression which reflects the trimming of the upper-fan coastal cliff (Figs. 9 and 10c). This marine episode resulted also in trimming of the alluvial incision cliff and the development of the sub-horizontal bench in early upper-fan deposits at about the sea-level of the time (c. -72 m) (see yellow dashed line on the river cliff in Fig. 3; Figs. 9 and 10c). This allowed up to 10,000 years for upper-fan deposition and incision before the fan is trimmed by the sea during the high sea-level peak at c. 39 kyr.

10 Lower-fan deposition (Figs. 10d) followed soon after the upper-fan marine trimming episode (Fig. 9). The relatively high sea-level at 37 kyr (c. -75 m; see Fig. 9) promoted fan deposition and the deteriorating climatic conditions, involving episodically increased river flow/carrying capacity, have increased sediment supply. Lower-fan deposits lapped up against cliffs cut in upper-fan deposits by alluvial incision along the Klados River and by the marine trimming sub-parallel to the modern shoreline (Fig. 10d). Lower-fan abandonment through incision commenced at ~36 kyr (LF-2a/b sample; Table 1).
15 We argue that the lower-fan surface was abandoned (Fig. 10e) sometime between ~36 kyr and 29 kyr due to river incision forced by the falling sea-level (that continued until ~18 kyr) (Fig. 9).

Marine trimming of the lower-fan is unlikely to have occurred between deposition and the last glacial maximum (~18 kyr), as sea-level progressively declined during that period. Following 18 kyr, sea-level rose rapidly by ~100 m in less than 10 kyr (Fig. 9). The Holocene high sea-level stand is the most likely candidate period for the marine trimming of the lower-fan (although we cannot constrain the initiation of the backward trimming of the lower-fan, the sea is likely to have shaped the current marine cliff c. 4-5 kyr ago; Fig. 10f). Between 18 kyr and 5 kyr BP, while sea-level was rising fast, tectonic uplift must have affected Domata, outpacing the rising sea-level and protecting the entire sequence from marine inundation and destruction. Immediately prior to the co-seismic uplift that affected western Crete at 1.5-2 kyr (Pirazzoli et al., 1982), the foot of the lower marine cliff would have been within the intertidal zone. Today, due to this earthquake uplift that generated a prominent stranded paleoshoreline (Figs. 6b and 10g), the foot of the lower marine-cliff is up to ~5 m above sea-level and may not currently be actively trimmed. We interpret a low terrace riser at about this elevation near the mouth of the Klados River (see middle red dashed line in Fig. 6b) to be relict from the channel of that time and the river channel downcutting a response to that first-millennium earthquake uplift.

30 In summary, deposition of the upper and lower-fan deposits was controlled by a marine base level and, in both cases, fan incision followed due to falling sea-level. The deposition of the upper-fan was largely completed by ~45 kyr BP, during a period of relative high sea-level (c. -70 m), and fan incision resulting in surface abandonment occurred between c. 45 and 40 kyr. Marine trimming of the upper-fan deposits occurred during a sea-level high (c. -72 m) at c. 39 kyr. Lower-fan deposition



was initiated soon afterwards and fan surface abandonment occurred between 36 and 29 kyr. The age of the sandy unit that mantles both the upper- and the lower-fan is ~25 kyr (UF-2; Fig. 9 and Table 1), postdating both fans as it was expected by their stratigraphic relation (silty sand that mantles both the lower and upper-fan).

5 The importance of tectonic uplift at Domata

The fan sequence at Domata provides a unique opportunity to link terrestrial deposition with sea-level fluctuations on southwestern Crete. Geomorphic analysis combined with dating shows that the development of the fan sequence can be accounted for by eustatic/climatic changes coupled with vertical tectonics. The latter can be rationalised if we consider that the landforms at Domata were formed 70 to 90 m below the current sea-level, implying that, unless tectonic uplift was significant, the entire sequence would have been inundated, and thus modified, by the rising sea-level during the last 20 kyr (Siddall et al., 2003). Therefore, a requirement for its preservation is that tectonic uplift rate outpaced the rising sea-level at any given time during the last ~40 kyr. A question that arises from this reasoning concerns the rate of the tectonic uplift at Domata and how it relates to the rate of rising sea-level. Dating key terrestrial and marginal marine geomorphological features would provide an average uplift rate for this part of Crete that could be compared to the rate of rising sea-level and also to other uplift rates on western Crete (which have been independently derived).

Our data show that the marine trimming episode at c. 39 kyr left a coastal cliff and cut an erosional intertidal bench in the upper-fan deposits (see yellow dashed line in Figure 3 and Figs. 9 and 10c). This marine bench provides an excellent datum upon which to estimate subsequent uplift. Indeed, a total uplift of 86 m is required between the marine trimming of the upper-fan materials (39 kyr when the sea-level was ca. -72m) and the present day to elevate the fan sequence to its current altitude of 14 m a.s.l. Thus, a minimum uplift rate required to bring this marine bench to its present day elevation is c. 2.2 mm/yr. Indeed, the plot in Figure 11 shows that with an average rate of ~2.2 mm/yr since formation (black line), the fan sequence would have escaped interaction with the wave-zone and, therefore, modification due to erosion (e.g., the black line of uniform uplift rate does not intersect the sea-level curve during the last 39 kyr). Independent support for similar uplift rate values comes from published radiocarbon ages on beachrock materials that mantle marine paleoshorelines in nearby localities: a calibrated radiocarbon age of 36,790 - 38,694 yrs BP from reworked rhodoliths in beachrock at an elevation of 10.5 m at Sougia, 9 km to the west of Domata, within a few thousand years of the proposed timing of marine trimming of the upper-fan, yields a required average uplift rate of 2.4 mm/yr (Mouslopoulou et al., 2015a). Similarly, beachrock on marine bench at 17 m elevation at Palaiochora, 20 km west of Domata, yields a calibrated radiocarbon age of 36,682 - 38,732 yrs BP, producing an average uplift rate of 2.5 mm/yr (Mouslopoulou et al., 2015a). Thus, the preservation and sub-aerial exposure of the landscape at Domata is due to the sufficient tectonic uplift that southern Crete experienced during late Quaternary.



In order to quantify the relative contribution of tectonics and eustasy on the formation of the landscape at Domata, here we compare published information on incremental uplift rates calculated by Mouslopoulou et al. (2015b) for western Crete over the last ~50 kyr with the uplift rate calculated for Domata over the last 39 kyr (c. 2.2 mm/yr; this study). Comparison shows that during the time period over which the key features at Domata formed (MIS 3), no significant uplift was accommodated on Crete as the region between ~20-45 kyr was experiencing a tectonically quiet period (Mouslopoulou et al., 2015b). Thus, the shaping of the landscape at Domata during MIS 3 must have been largely achieved by sea-level fluctuations. This comparison also suggests that ~80 m of uplift (subtracting 6m of late Holocene co-seismic uplift), have been accumulated sometime between 5 and 20 kyr BP, resulting in an average uplift rate of 5.3 mm/yr (Fig. 11; dashed red line). However, this uplift rate would have been insufficient to outpace the rising sea-level between 8 and 12 kyr BP (see dashed red line intersecting the sea-level curve in Fig. 11) and, thus, the fan sequence would have been inundated and eroded by the rising sea-level. This, in turn, implies that the uplift rate at Domata was higher than 5.3 mm/yr. We favour a scenario in which uplift was mostly accommodated by about 9 kyr BP, at an average of ~7 mm/yr (see solid red line in Fig. 11 that does not intersect the sea-level curve). Comparable uplift rates have been independently recorded at numerous localities on western and eastern Crete for the last 20,000 years by Shaw et al. (2008), Tiberti et al. (2014) and Mouslopoulou et al. (2015b).

Thus, the development and evolution (~50-20 kyr BP) of the suite of geomorphic features at Domata can be largely explained by eustatic sea-level fluctuations and sedimentation variations controlled by climatic conditions, without the requirement for significant vertical movements. However, it is the subsequent tectonic uplift that preserved and exposed sub-aerially the coastal geomorphic features.

6 Conclusions

Alluvial fans often provide a useful index with which to decode the information recorded on the landscape in complex tectonic settings, such as those of Eastern Mediterranean. Herein we use analysis of geomorphic landforms and OSL dating on a double alluvial-fan system in Crete, an island straddling the forearc of the Hellenic subduction margin, to constrain and quantify the factors responsible for its landscape evolution. Data analysis shows that sea-level fluctuations in response to varying climatic conditions formed the landscape at Domata during MIS 3 (57-29 kyr BP). It is, however, because of the tectonic uplift over the subsequent ~20 thousand years that the entire alluvial sequence escaped marine inundation and is preserved sub-aerially today. Thus, both eustasy and tectonism impacted on the formation and preservation of the landscape at Domata, but over temporally distinct time periods.

Acknowledgements



We thank our relative and friend Nikos Mouslopoulos and late Stavros Sartzetakis, respectively, for their generous help during fieldwork. We are grateful to the National Cadastre and Mapping Agency of Greece for providing, free of charge, digital elevation maps and imagery for building the DEM's in Figure 4.

5 Author's contributions

V.M, J.B., D.M and P.P conceived the research idea, pursued all associated fieldwork and analysis of the results. A.F. performed the OSL dating. O.O. provided guidance and contributed to the development of the ideas presented in this article. The manuscript was written collectively by all authors.

10 Competing interests

The authors declare that they have no conflict of interest

References

- Ammianus Marcellinus: translated by C.D. Yonge, 1862
- Angelier, J., Lyberis, N., Le Pichon, X., Barrier, E., and Huchon, P.: The tectonic development of the Hellenic Arc and the
15 sea of Crete: A synthesis, *Tectonophysics*, 86, 159-196, 1982.
- Antonioli, F., Anzidei, M., Lambeck, K., Auriemma, R., Gaddi, D., Furlani, S., Orrù, P., Solinas, E., Gaspari, A., Karinja, S.,
Kovačić, V., and Surace, L.: Sea-level change during the Holocene in Sardinia and in the northeastern Adriatic
(central Mediterranean Sea) from archaeological and geomorphological data, *Quatern. Sci. Rev.*, 26, 2463-2486,
2007.
- 20 Balescu, S., and Lamothe, M.: Comparison of TL and IRSL age estimates of feldspar coarse grains from waterlain
sediments, *Quatern. Geochron.*, 13, 437-444, 1994.
- Bassinot, F. C., Labeyrie, L. D., Vincent, E., Quidelleur, X., Shackleton, N. J., and Lancelot, Y.: The astronomical theory of
climate and the age of the Brunhes-Matuyama magnetic reversal, *Earth Planet. Sci. Lett.*, 126, 91-108, 1994.
- Blair, M. W., Yukihiro, E. G., and McKeever, S. W. S.: Experiences with single-aliquot OSL procedures using coarse-grain
25 feldspars, *Radiat. Measur.*, 39, 361 - 374, 2005.
- Chappell, J., Omura, A., Esat, T., McCulloch, M., Pandolfi, J., Ota, Y., and Pillans, B.: Reconciliation of late Quaternary sea
levels derived from coral terraces at Huon Peninsula with deep sea oxygen isotope records, *Earth Planet. Sci. Lett.*,
141, 227-236, 1996.
- Christodoulou, G.E., and Tataris, A. A.: Geological map of Greece, Alikianou Sheet Scale 1:50 000, Institute of Geological
30 and Subsurface Research, Greece, 1969.
- Dickinson, W. R.: Paleoshoreline record of relative Holocene sea levels on Pacific islands, *Earth Sci. Rev.*, 55, 191-234,
2001.



- FAO: World reference base for soil resources, World Soil Resources Reports No. 103, 2nd edn. Food and Agriculture Organization of the United Nations, FAO, Rome, 2006.
- Galbraith, R. F., and Roberts, R. G.: Statistical aspects of equivalent dose and error calculation and display in OSL dating: An overview and some recommendations, *Quatern. Geochr.*, 11, 1-27, 2012.
- 5 Gallen, S. F., Wegmann, K. W., Bohnenstiehl, D. R., Pazzaglia, F. J., Brandon, M. T., and Fassoulas, C.: Active simultaneous uplift and margin-normal extension in a forearc high, Crete, Greece, *Earth Planet. Sci. Lett.*, 398, 11–24, 2014.
- Huntley, D. J., and Baril, M. R.: The K content of the K-feldspars being measured in optical dating or in thermoluminescence dating, *Ancient TL*, 15, 11-13, 1997.
- 10 Imbrie, J., Hays, J. D., Martinson, D. G., McIntyre, A., Mix, A. C., Morley, J. J., Pisias, N. G., Prell, W. L., and Shackleton, N. J.: The orbital theory of Pleistocene climate: support from a revised chronology of the marine $\delta^{18}\text{O}$ record: In “Milankovitch and climate”, A.L. Berger (Ed.), Part 1, 269-305, 1984.
- Lambeck, K., and Purcell, A.: Sea-level change in the Mediterranean Sea since the LGM: model predictions for tectonically stable areas, *Quatern. Sci. Rev.*, 24, 1969-1988, 2005.
- 15 Le Pichon, X., and Anglier, J.: The Hellenic arc and trench system: a key to the neotectonic evolution of the eastern Mediterranean area, *Tectonophysics*, 60, 1-42, 1979.
- Le Pichon, X., and Anglier, J.: The Aegean Sea, *Phil. Trans. R. Soc. A.*, 300, 357-372, 1981.
- Lair, G. J., Zehetner, F., Hrachowitz, M., Franz, N., Maringer, F. J., and Gerzabek, M. H.: Dating of soil layers in a young floodplain using iron oxide crystallinity, *Quatern. Geochron.*, 4, 260–26, 2009.
- 20 Martinson, D. G., Pisias, N. G., Hays, J. D., Imbrie, J., Moore, T. C., and Shackleton, N. J.: Age dating and the orbital theory of the ice ages: Development of a high-resolution 0 to 300,000-year chronostratigraphy, *Quatern. Res.*, 27, 1-29, 1987.
- Masclé J., Le Cleach’h, A., and Jongsma, D.: The eastern Hellenic margin from Crete to Rhodes: example of progressive collision, *Mar. Geol.*, 73, 145-168, 1986.
- 25 Meier, T., Becker, D., Endrun, B., Bohnhoff, M., Stöckert, B., and Harjes, H.-P.: A model for the Hellenic subduction zone in the area of Crete based on seismological investigations, *Geol. Soc. Lond.*, 291, 183–199, 2007.
- Meulenkamp, J. E., van der Zwaan, G. J., and vanWamel, W. A.: On late Miocene to recent vertical motions in the Cretan segment of the Hellenic arc, *Tectonophysics*, 234, 53–72, 1994.
- Moraetis, D., Mouslopoulou, V., and Pratikakis, A.: Sorption of the Rare Earth Elements and Yttrium (REE-Y) in calcite: the mechanism of a new effective tool in identifying paleoearthquakes on carbonate faults, v. 17, EGU2015-3437, 2015.
- 30 Mouslopoulou, V., Begg, J., Nicol, A., Oncken, O., and Prior, C.: Formation of Late Quaternary paleoshorelines in Crete, Eastern Mediterranean, *Earth Planet. Sci. Lett.*, 431, 294-307, 2015a.
- Mouslopoulou, V., Nicol, A., Begg, J., Oncken, O., and Moreno, M.: Clusters of mega-earthquakes on upper plate faults control the Eastern Mediterranean hazard, *Geophys. Res. Lett.*, 42, 10282–10289, 2015b.



- Mourtzas, N. D.: Fish tanks of eastern Crete (Greece) as indicators of the Roman sea-level, *J. Archaeol. Sci.*, 39, 2392-2408, 2012.
- Murray, A. S., and Wintle, A. G.: Luminescence dating of quartz using an improved single-aliquot regenerative-dose protocol, *Radiat. Measur.*, 32, 57-73, 2000.
- 5 Murray, A. S., and Wintle, A. G.: The single aliquot regenerative dose protocol: potential for improvements in reliability, *Radiat. Measur.*, 37, 377-381, 2003.
- Nemec, W., and Postma, G.: Quaternary alluvial fans in southwestern Crete: sedimentation processes and geomorphic evolution. In: Marzo, M., Puigdefábregas, C. (Eds.), *Alluvial Sedimentation*, Sp.Publ. Intern. Assoc. Sediment., 17, 235–276, 1993.
- 10 Papadimitriou, E., and Karakostas, V.: Rupture model of the great AD 365 Crete earthquake in the southwestern part of the Hellenic Arc, *Acta Geophys.*, 56, 293-312, 2008.
- Papazachos B. C., and Papazachou C.: *The earthquakes of Greece*, Ziti publications, Thessaloniki, Greece, 286 pp. (in Greek), 2003.
- Papazachos, C. B., Karakaisis, G. F., Scordilis, E. M., and Papazachos, B. C.: New observational information on the precursory accelerating and decelerating strain energy release, *Tectonophysics*, 423, 83–96, 2006.
- 15 Peters, J. M., Troelstra, S. R., and van Harten, D.: Late Neogene and Quaternary vertical movements in eastern Crete and their regional significance, *J. Geol. Soc.*, 142, 501-513, 1985.
- Pirazzoli, P. A., Thommeret, J., Thommeret, Y., Laborel, J., and Montag-Gioni, L. F.: Crustal block movements from Holocene shorelines: Crete and Antikythira (Greece), *Tectonophysics*, 86, 27–43, 1982.
- 20 Pirazzoli, P. A., Laborel, J., and Stiros, S. C.: Earthquake clustering in the Eastern Mediterranean during historical times, *J. Geophys. Res.*, 101, 6083–6097, 1996.
- Pope, R., Wilkinson, K., Skourtsos, E., Triantaphyllou, M., and Ferrier, G.: Clarifying stages of alluvial-fan evolution along the Sfakian piedmont, southern Crete: New evidence from analysis of post-incisive soils and OSL dating, *Geomorphology*, 94, 206-225, 2008.
- 25 Prescott, J.R., and Hutton, J.T.: Cosmic ray contributions to the dose rates for luminescence and ESR dating: Large depths and long-term time variations, *Radiat. Measur.*, 23, 497-500, 1994.
- Preusser, F., Ramseier, K., and Schlüchter, C.: Characterisation of low OSL intensity quartz from the New Zealand Alps, *Radiat. Measur.*, 41, 871-877, 2006.
- Rabineau, M., Berne, S., Aslanian, D., Olivet, J-L., Joseph, P., Guillocheau, F., Bourillet, J-F., Ledrezen, E., and Granjeon, D.: Sedimentary sequences in the Gulf of Lion: A record of 100,000 years climatic cycles, *Mar. Petrol. Geol.*, 22, 775–804, 2005.
- 30 Reilinger, R., McClusky, S., Paradissis, D., Ergintav, S., and Vernant, P.: Geodetic constraints on the tectonic evolution of the Aegean region and strain accumulation along the Hellenic subduction zone, *Tectonophysics*, 488, 22-30, 2010.



- Roberts, G. G., White, N. J., Shaw, B.: An uplift history of Crete, Greece, from inverse modelling of longitudinal river profiles, *Geomorphology*, 198, 177–188, 2013.
- Ryan, W. B. F., Stanley, D. J., Hersey, J. B., Fahlquist, D. A., and Allan, T. D.: The tectonics and geology of the Mediterranean Sea., in: A Maxwell (Editor), *The Sea*, 4, II, Wiley-Interscience, New York, N.Y., 387-492, 1970.
- 5 Shaw, B., Ambraseys, N. N., England, P. C., Floyd, M. A., Gorman, G. J., Higham, T. F. G., Jackson, J. A., Nocquet, J.-M., Pain, C. C., Piggott, and M. D.: Eastern Mediterranean tectonics and tsunami hazard inferred from the AD 365 earthquake, *Nat. Geosci.*, 1, 268–276, 2008.
- Siddall, M., Rohling, E. J., Almogi-Labin, A., Hemleben, Ch., Meischner, D., Schmelzer, I., and Smeed, D. A.: Sea-level fluctuations during the last glacial cycle, *Nature*, 423, 853–858, 2003.
- 10 Soil Atlas of Europe, European Soil Bureau Network European Commission: Office for Official Publications of the European Communities, L-2995 Luxembourg, pp. 128, 2005.
- Stefanakis, M. I.: Western Crete: From Captain Spratt to modern archaeoseismology, *Geolog. Soc. Am. Sp. Pap.*, 471, 67-79, 2010.
- Steffen, D., Preusser, F., and Schlunegger, F.: OSL quartz age underestimation due to unstable signal components, *Quatern. Geochron.*, 4, 353-362, 2009.
- 15 Stiros, S.C.: The AD 365 Crete earthquake and possible seismic clustering during the fourth to sixth centuries AD in the Eastern Mediterranean: a review of historical and archaeological data, *J. Struct. Geol.*, 23, 545–562, 2001.
- Stiros, S.: The 8.5+ magnitude, AD 365 earthquake in Crete: Coastal uplift, topography changes and archaeological and historical signature, *Quatern. Intern.*, 216, 54-63, 2010.
- 20 Strasser, T. F., Runnels, C., Wegmann, K., Panagopoulou, E., McCoy, F., Digregorio, C., Karkanis, P., and Thompson, N.: Dating Palaeolithic sites in southwestern Crete, Greece, *J. Quatern. Sci.*, 26, 553–560, 2011.
- Strobl, M., Hetzel, R., Fassoulas, C., and Kubik, P.W.: A long-term rock uplift rate for eastern Crete and geodynamic implications for the Hellenic subduction zone, *J. Geodyn.*, 78, 21-31, 2014.
- Tiberti, M. M., Basili, R., Vannoli P.: Ups and downs in western Crete (Hellenic subduction zone), *Sci. Rep.*, 4, 5677, 1-7, 25 2014.
- Vernant, P., Reilinger, R., and McClusky, S.: Geodetic evidence for low coupling on the Hellenic subduction plate interface, *Earth Planet. Sci. Lett.*, 385, 122-129, 2014.
- Wallinga, J., Murray, A., and Wintle, A.: The single-aliquot regenerative-dose (SAR) protocol applied to coarse-grain feldspar, *Radiat. Measur.*, 32, 529-533, 2000.
- 30 Wang, X., Wenfeng Tan, F. L., Xionghan Feng, W. L., and Sparks, D. L.: Characteristics of Phosphate Adsorption-Desorption Onto Ferrihydrite: Comparison With Well-Crystalline Fe (Hydr)Oxides, *Soil Sci.*, 178, 1-11, 2013.
- Waters, J. V., Jones, S. J., and Armstrong, H. A.: Climatic controls on late Pleistocene alluvial fans, Cyprus, *Geomorphology*, 115, 228-251, 2010.



Zacharias, N., Bassiakos, Y., Hayden, B., Theodorakopoulou, K., and Michael, C.: Luminescence dating of nearshore deltaic deposits from Eastern Crete, Greece, *Geomorphology*, 109, 46-53, 2009.

Figure captions

Figure 1: Map illustrating the location of Crete within the forearc of the Hellenic subduction margin. The locations of the Hellenic Trough and its splays (the Ptolemy, Pliny and Strabo troughs) are indicated. Numbered arrows show geodetically-derived convergence rates between the African and Eurasian plates and their azimuths at selected sites (after Reilinger et al., 2010). The study area at Domata is indicated by white filled circle while the regions of Sfakia (S), Elafonisi (E), Palaiochora (P) and Agios Georgios (AG) are marked with yellow circles. WG=White Mountains. Hillshade is derived from GeoMapApps.

10

Figure 2: Northward view of the beach at Domata illustrating the two generations of fan surfaces and their separate episodes of marine trimming. The location of the Klados gorge, the two elevated marine benches cut on bedrock and the 365 AD uplifted shoreline are indicated.

Figure 3: The fan sequence at Domata looking obliquely towards southeast. The two fan surfaces and their respective stream-incised cliffs are illustrated. The yellow dashed line in the present stream cliff indicates the benched upper-fan erosional surface, which is overlain by the deposits of the lower-fan. This marker was used to calculate a long-term (39 kyr) uplift rate at Domata (see text for details). White spots mark the location of OSL samples.

Figure 4: a) Digital elevation model of the study area at Domata as viewed obliquely from the southwest. The model is derived by using the nearest neighbour algorithm along with the GPS measurements marked and colour coded by 10 m elevation bands. Note the upper and lower-fan surfaces, each incised following surface abandonment, and each trimmed by marginal marine processes. b) Digital elevation model with National Greek Cadastre Agency orthophoto draped, along with the GPS measurements. Yellow polygon depicts the area illustrated in the DEM of panel (a). Red polygons indicate the localities of the profiles of Figure 5.

Figure 5: Profiles of fan surfaces projected onto common planes parallel with the modern Klados River channel (above) and parallel with the modern coastline (below). Horizontal and vertical scales for each profile are similar, with a VE of c. 1.25. Note that the downstream slope of the upper and lower-fan surfaces are about the same, both a little steeper than the slope of the modern stream channel. Also note that the upper-fan surface slopes less to the east than the lower-fan surface, so that the upper-fan marine cliff is higher at the eastern end of the beach than at the west. The highest elevation of the lower-fan surface is close to the foot of the incision of the upper-fan, while the upper-fan surface is highest at its incision point.



Figure 6: **a)** The present marine cliff at Domata (above), annotated to highlight various sedimentary relationships (below). The cliff comprises mostly moderately bedded gravels of the lower-fan sequence. The lower contact of the lower-fan gravels (white dashed line) is irregular, but sub-horizontal and lower-fan bedding (white dotted lines) laps onto it. Some individual horizons within the lower-fan deposits can be traced laterally for 100's metres, but channelling, bed-lensing and pinch-outs are present. Note also that the exposed marine cliff beneath the upper-fan surface (behind the forested lower-fan surface). **b)** Looking west across the Klados River mouth (foreground), the uplifted shoreline attributed to the 1.5-2 kyr BP earthquake sequence (dashed red line, left) aligns well with a low terrace riser on the west side of the river (dashed red line, middle). Incision of the stream below the surfaces is attributable to post-earthquake adjustment to new base levels. Note sea-cliffing of all terrace surfaces. A probable higher terrace riser is marked with fine dotted white line.

Figure 7: Individual OSL ages for all selected aliquots and resulting kernel density estimates. Mean = arithmetic mean, sd = standard deviation (relative and absolute; shaded area), se = standard error (relative and absolute). KDE_{max} = empirical estimate of the probability density function of the observed age distribution. Shaded area: standard deviation.

Figure 8: **a)** The two alluvial fans with their tree cover (*Pinus brutia*). Arrows indicate the soil-cover that develops on each of the fan surfaces. **b)** The soil development on the lower-fan (LF) surface is ~12 cm (from 14 to 26 cm, as indicated by the white arrows). **c)** The soil development on the upper-fan (UF) surface is ~40 cm (from 16 to 56 cm, as indicated by the white arrows). The parent rock in both cases is indicated.

Figure 9: The OSL chronology of the geomorphic features at Domata plotted against a simplified version of the global sea-level curve after Siddall et al. (2003). The shaded zone in the background represents Siddall et al.'s stated error range. Large filled circles represent means of OSL dates, small filled circles medians and the bars are error bars (at 1σ). The geomorphic event sequence described in the text is shown above the figure and the favoured of three alternative high sea-level stands within MIS 3 to have trimmed the upper-fan surface prior to lower-fan deposition, is identified with a solid vertical blue line at 39 kyr BP.

Figure 10: The sequence of events that contributed to the development of the landscape at Domata is schematically illustrated: a) Upper-fan deposition due to sea-level high stand (base level); b) Abandonment of the upper-fan surface due to falling sea-level; c) Sea-level rise resulting in the trimming of the upper-fan deposits and cutting a marine bench; d) Lower-fan deposition starts during relatively high sea-level, and laps against both the river incision cliff and the coastal cliff in the upper-fan; e) As sea-level falls, the lower-fan surface is abandoned through entrenchment; f) A return to high sea-level results in coastal trimming of the lower-fan deposits; g) One or more earthquakes in the first millennium AD resulted in 6 m



of uplift at Domata and corresponding adjustments to the lower Klados River geomorphology. The approximate chronology of each stage is annotated.

Figure 11: The plot discusses the required uplift rate to elevate the marine cliff/bench of the upper-fan from its elevation at genesis (39 kyr BP) to its present elevation (+14 m). The simplified sea-level curve (after Siddall et al., 2003) is illustrated by thick blue line. The black line represents a constant uplift rate of 2.2 mm/yr (established in this study). The red dashed line represents a minimum uplift rate for Domata of ~5.3 mm/yr tailored to empirical data (Mouslopoulou et al., 2015b). The red solid line represents an uplift rate of ~ 7 mm/yr (see text for details).

10 **Table 1:** OSL dosimetry measurements and IRSL ages (potassium feldspar).

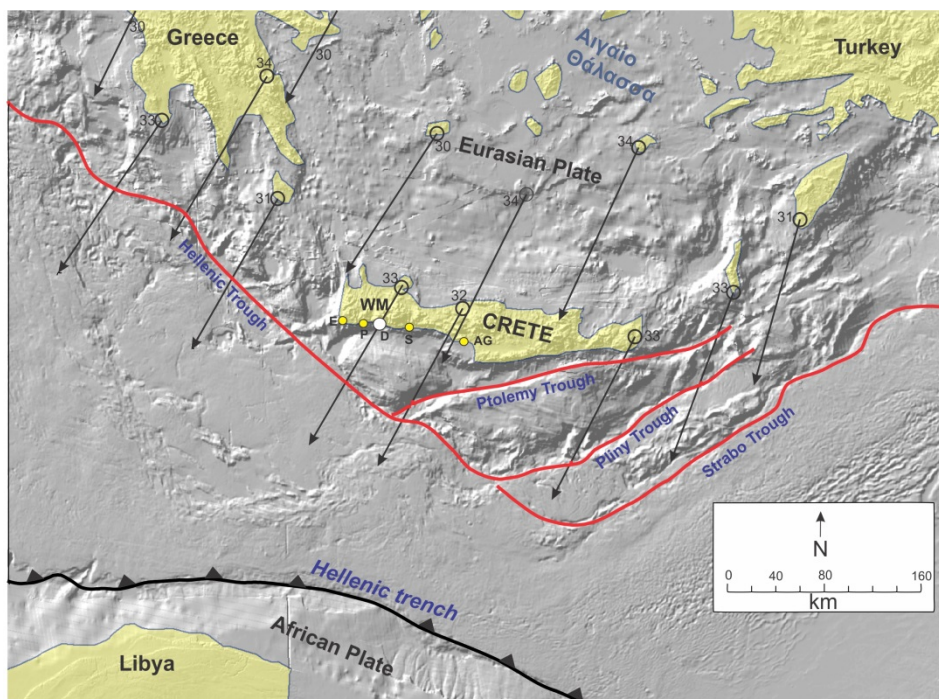


Figure 1

5

10

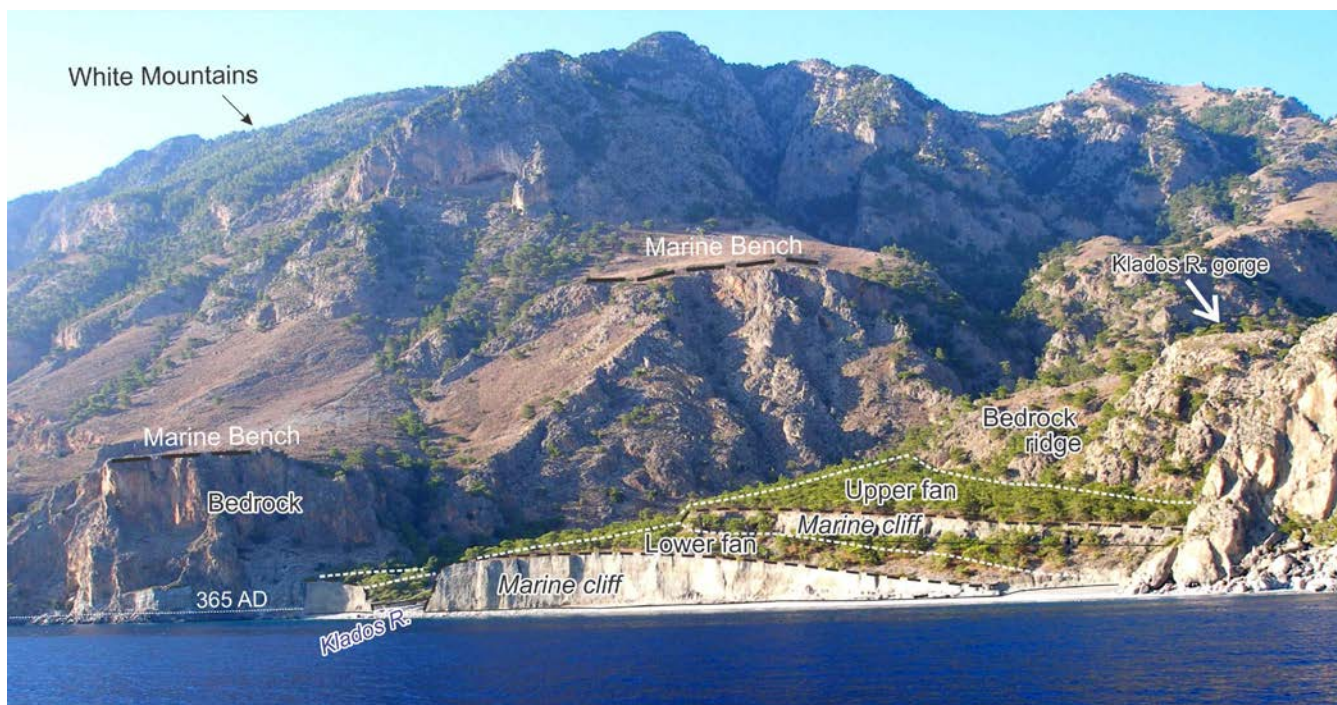


Figure 2

5

10



Figure 3

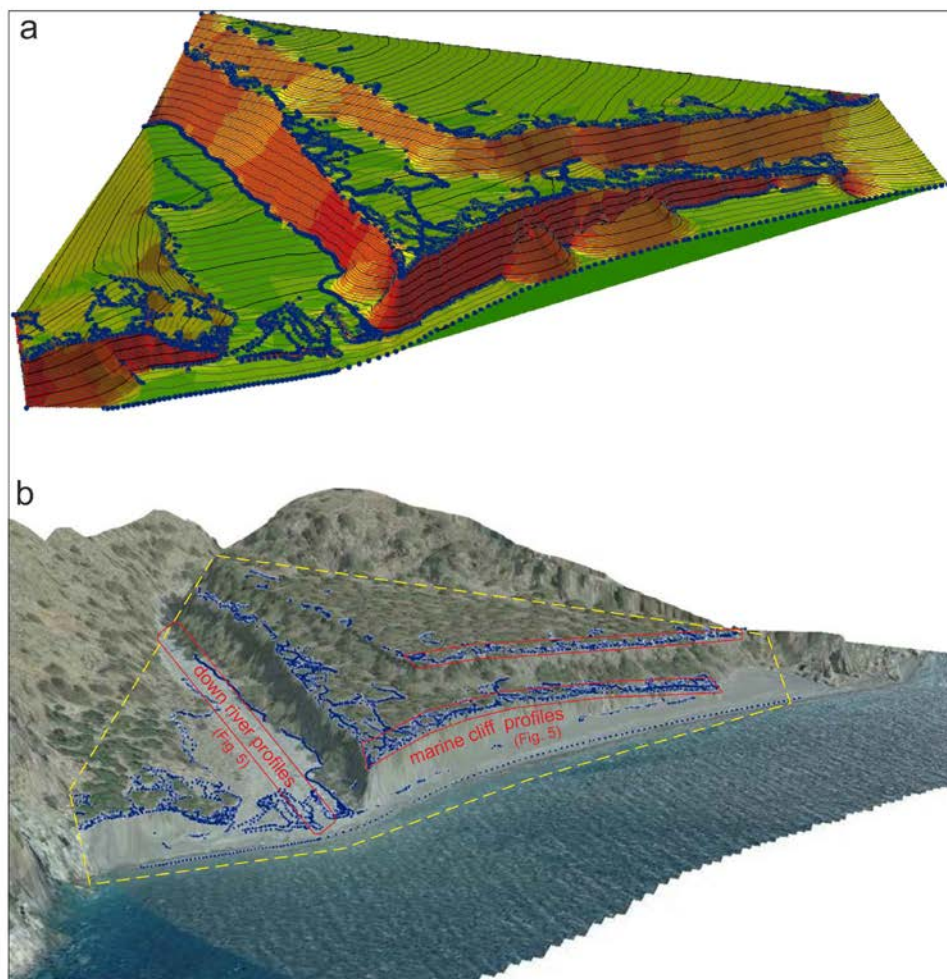


Figure 4

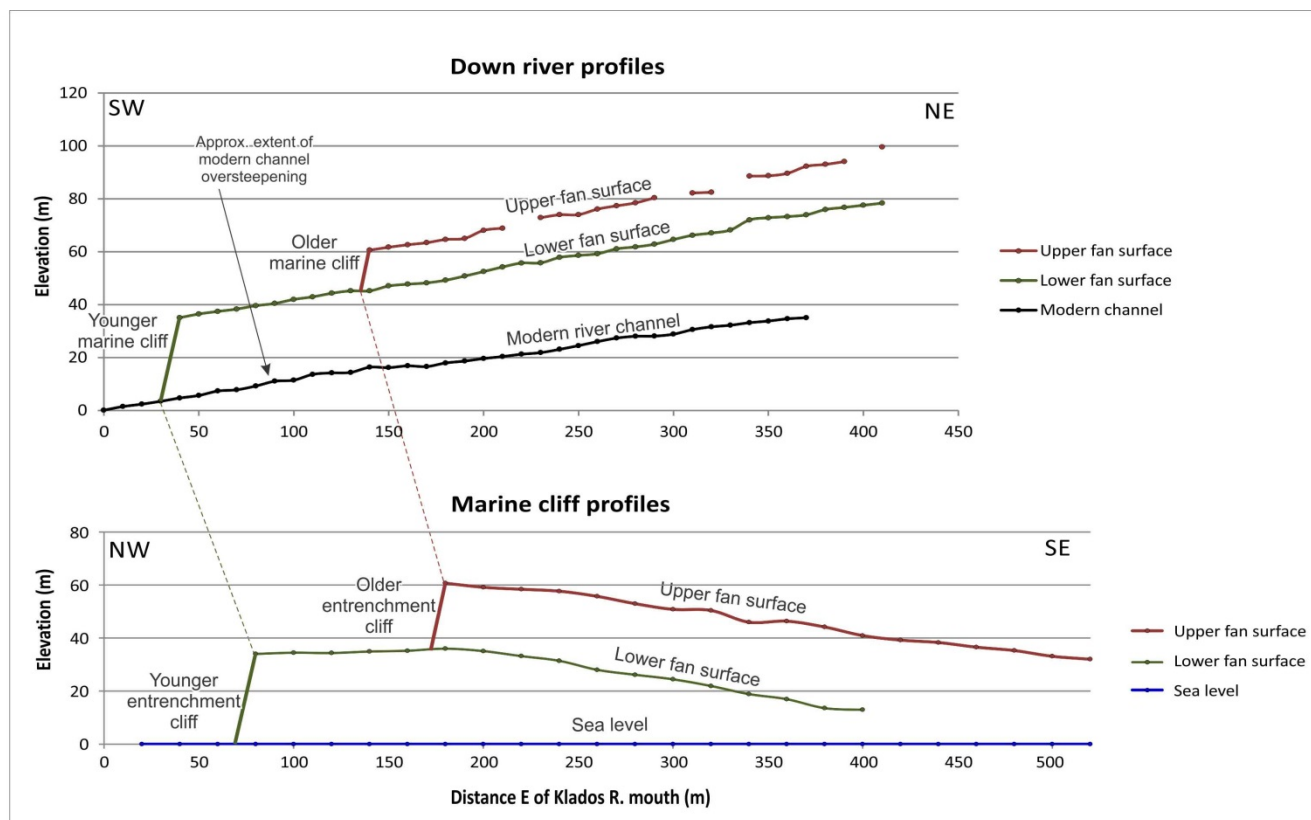


Figure 5

5

10



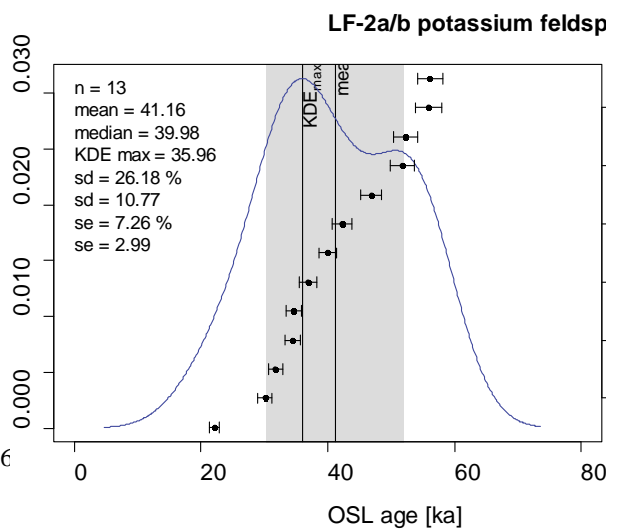
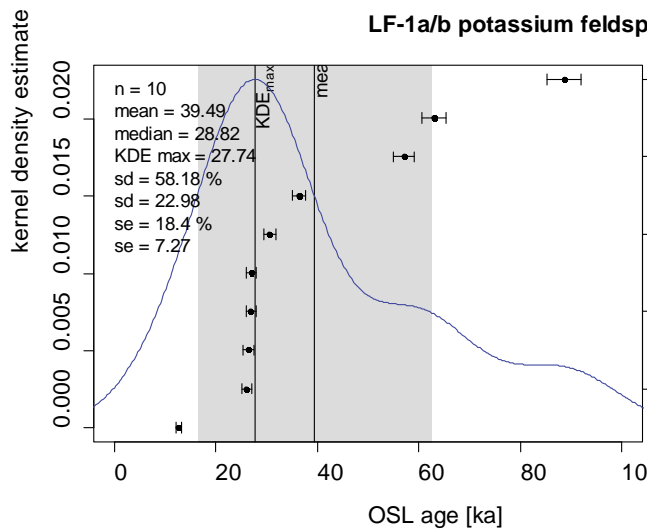
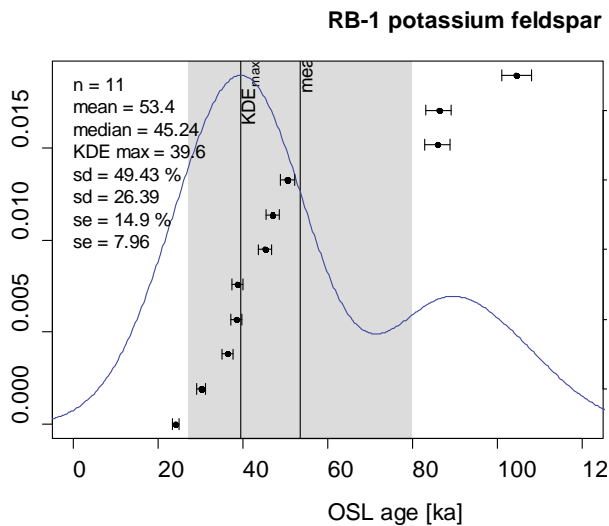
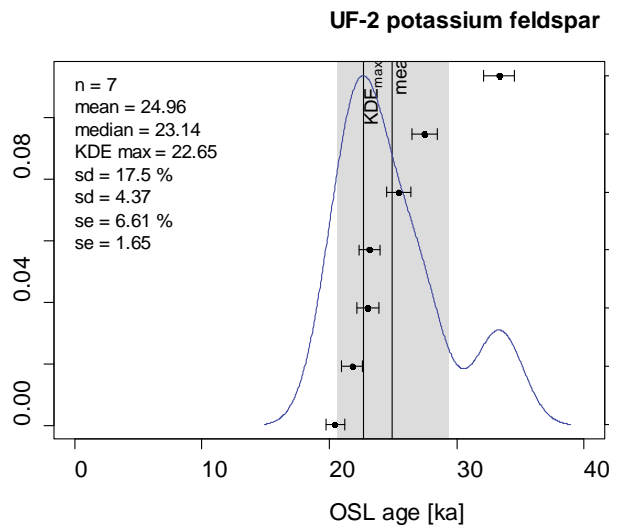
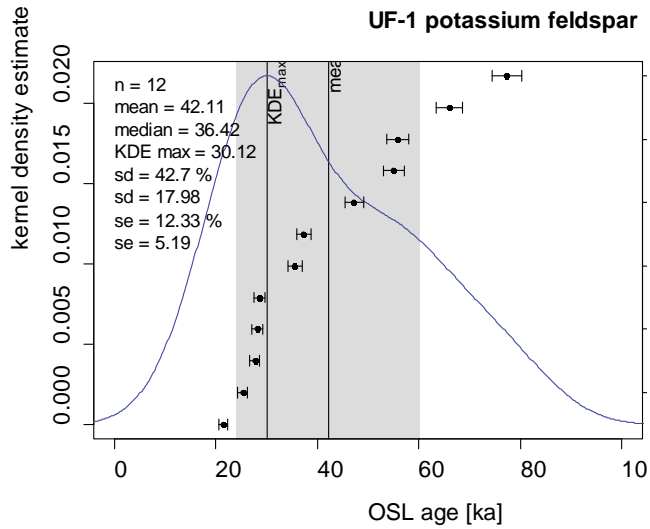
Figure 6

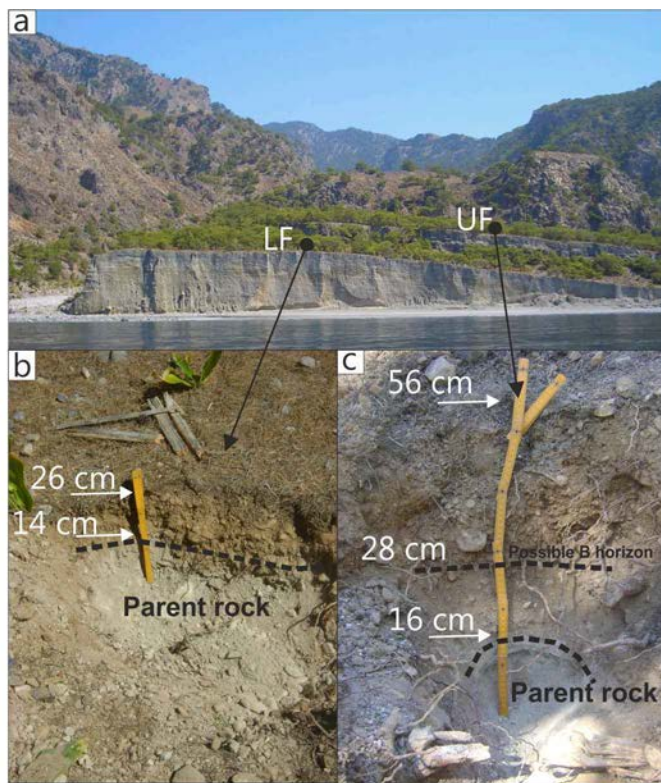
5

10



OSL age distributions





5 Figure 8

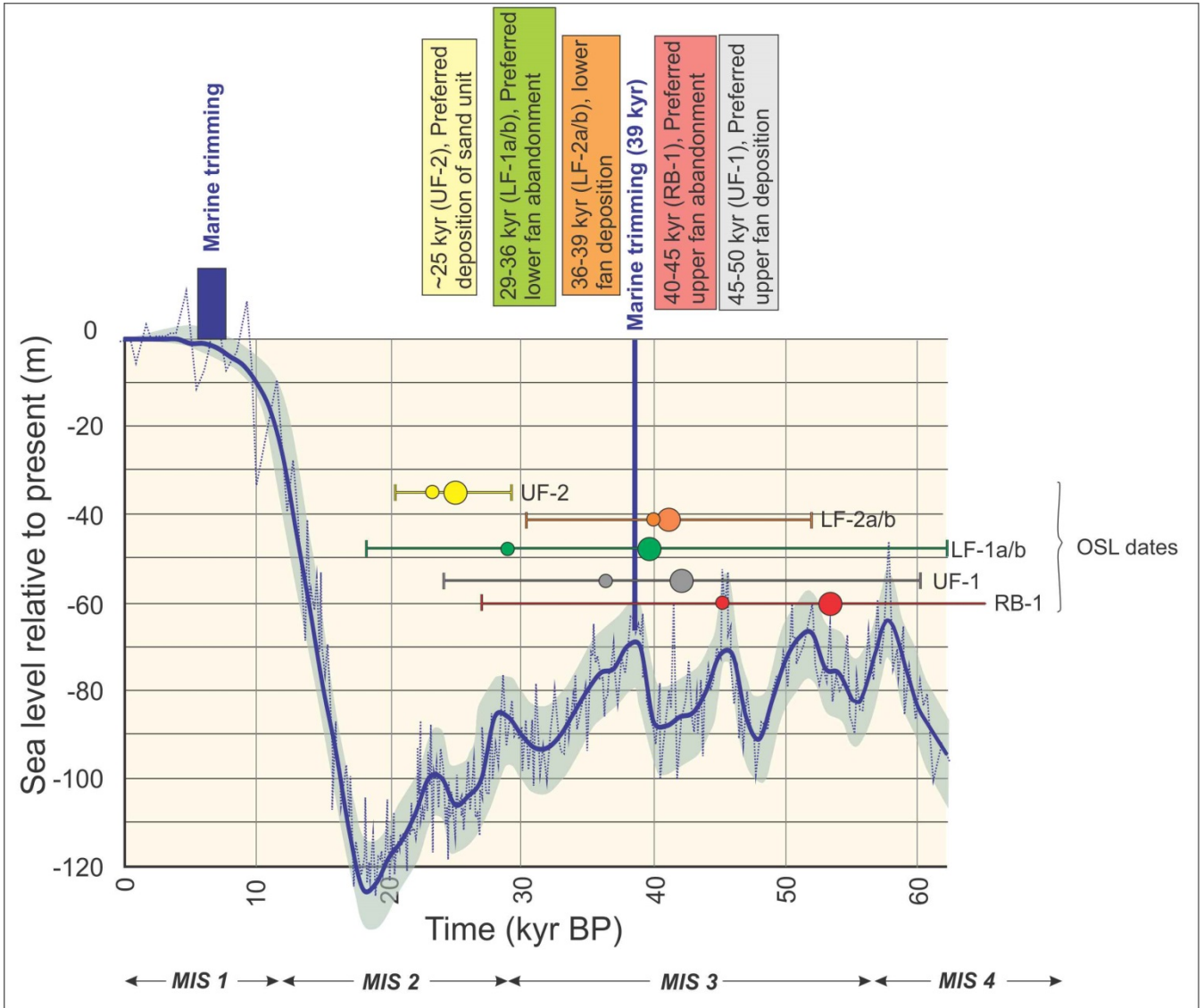


Figure 9

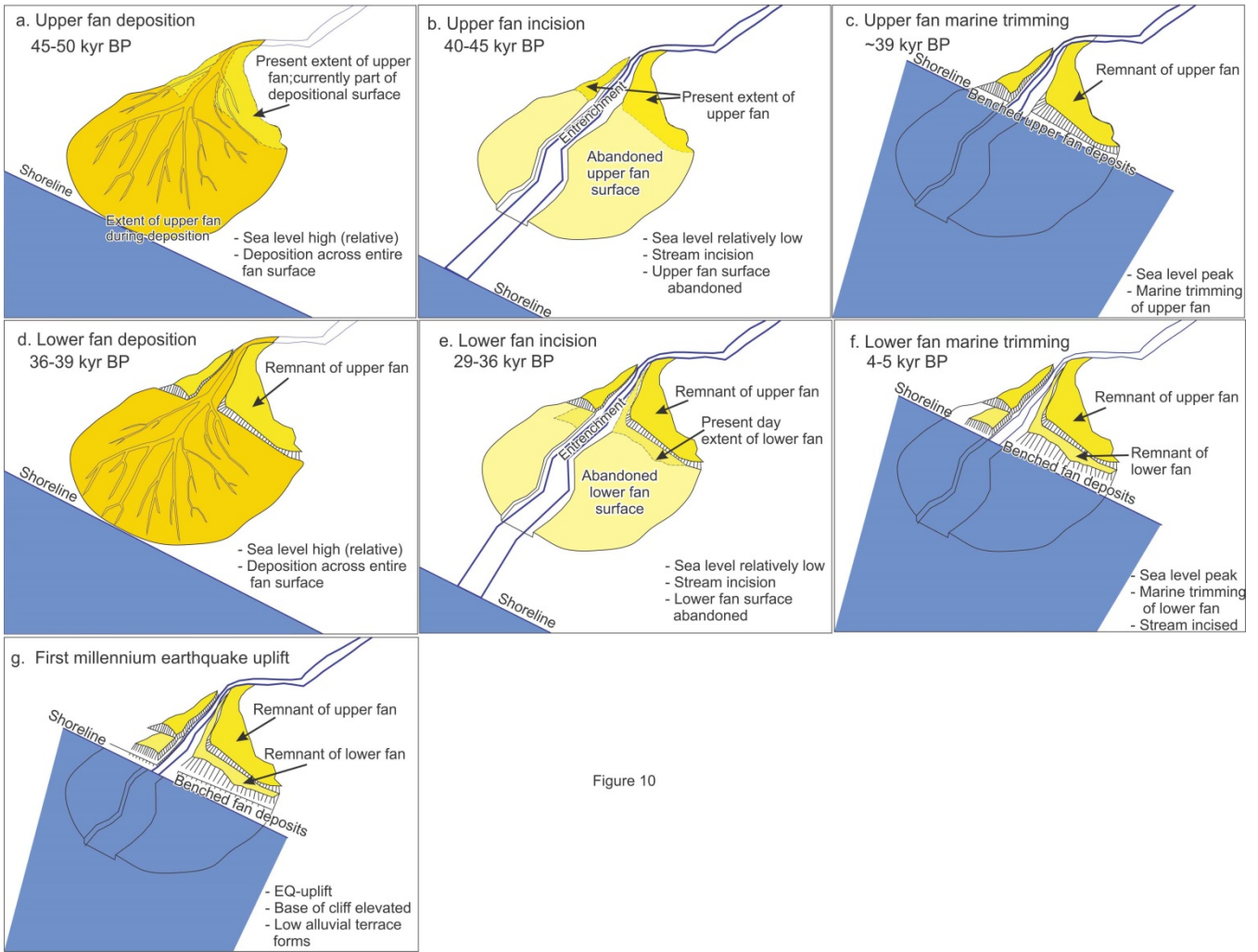


Figure 10

5

10

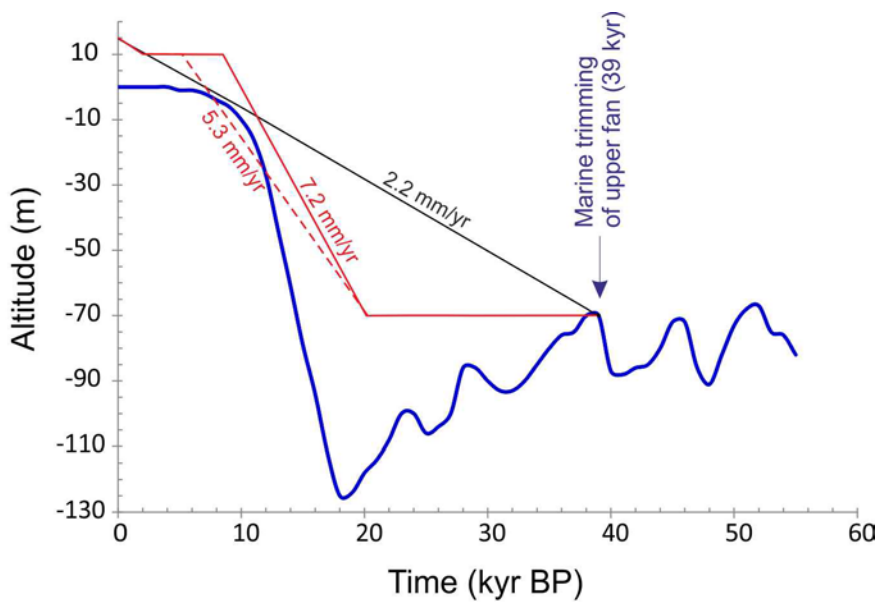


Figure 11

5

10



Sample (depth)	Easting	Northing	Altitude (m)	Lab. no. (aliquot no.)	U	Th	K	Cosmic dose	Water cont.	Water cont.	Dose rate (D ₀)	Equivalent dose (D _e) [Gy]			Standard deviation	Standard error (g)
					[ppm]	[ppm]	[%]	[mGy/ka]	[%]	[%]	[Gy/ka]	IRSL age [ka]			[%]	[%]
					(a)	(a)	(a)	(b)	(c)	(d)	(e)	Mean	Median	KDE max (f)	[ka]	[ka]
UF-1 (0.3 m)	023° 54' 50.9"	35° 13' 47.8"	84	HUB-0423 (12)	0.46 ± 0.02	0.63 ± 0.06	0.11 ± 0.01	195 ± 20	1,1	3 ± 2	0.99 ± 0.07	41.7 Gy	36.0 Gy	29.8 Gy	42,7%	12,3%
												42.1 ka	36.4 ka	30.1 ka	18.0 ka	5.2 ka
UF-2 (1.1 m)	023° 54' 56.9"	35° 13' 35.9"	30	HUB-0424 (7)	1.06 ± 0.04	2.36 ± 0.13	0.53 ± 0.01	173 ± 17	5,1	5 ± 2	1.67 ± 0.11	41.7 Gy	38.6 Gy	37.8 Gy	17,5%	6,6%
												25.0 ka	23.1 ka	22.7 ka	4.4 ka	1.7 ka
RB-1 (28.0 m)	023° 54' 41.1"	35° 13' 44.5"	14	HUB-0425 (11)	0.84 ± 0.02	0.62 ± 0.05	0.15 ± 0.01	17 ± 2	1,6	3 ± 2	0.96 ± 0.06	51.3 Gy	43.4 Gy	38.0 Gy	49,4%	14,9%
												53.4 ka	45.2 ka	39.6 ka	26.4 ka	8.0 ka
LF-1a/b (0.28 m)	023° 54' 44.1"	35° 13' 45.1"	43	HUB-0426 (10)	0.67 ± 0.02	0.4 ± 0.05	0.09 ± 0.01	194 ± 19	0,3	3 ± 2	1.01 ± 0.07	39.9 Gy	29.1 Gy	28.0 Gy	58,2%	18,4%
												39.5 ka	28.8 ka	27.7 ka	23.0 ka	7.3 ka
LF-2a/b (0.24 m)	023° 54' 43.8"	35° 13' 41.9"	46	HUB-0427 (13)	0.73 ± 0.02	0.67 ± 0.04	0.1 ± 0.01	195 ± 20	1,3	3 ± 2	1.07 ± 0.07	44.0 Gy	42.8 Gy	38.5 Gy	26,2%	7,3%
												41.2 ka	40.0 ka	36.0 ka	10.8 ka	3.0 ka
(a)	Uranium, thorium, and potassium contents were determined via high resolution gamma ray spectrometry (HPGe detector). U-238: U-234 (53.2 keV), Th-234 (63.3 keV), Ra-226 (186.1 keV), Pb-214 (295.2 keV, 351.9 keV), Bi-214 (609.3 keV, 1120.3 keV, 1764.5 keV), Pb-210 (46.5 keV). Th-232: Ac-228 (338.3 keV, 911.2 keV, 969.0 keV), Pb-212 (238.6 keV), Bi-212 (727.3 keV), Tl-208 (583.2 keV). K-40: 1461.0 keV. U-238 and Th-232: The arithmetic means of the activities of the above mentioned natural daughter products were used (± standard error). The internal K content of the potassium feldspar was set to 12.5 ± 0.5 % (Huntley & Baril 1997).															
(b)	Cosmic dose rates were estimated regarding geographic position (35°N, 24°E), altitude and sampling depth.															
(c)	Water content of sediment samples in % of dry mass (oven dried for 24 h at 105 °C).															
(d)	Water content used for dose rate calculation.															
(e)	For coarse grain potassium feldspar an a-value of 0.15 ± 0.05 was assumed (Balescu & Lamothe 1994).															
(f)	KDE max: Maximum density of the kernel density estimation.															
(g)	Standard error of the mean: standard deviation divided by the square root of the number of measured aliquots.															

Table 1